Effects of ordered islands on surface resistivity: Ni on Au(111)

Joshua I. Cohen and R. G. Tobin[a)]
Department of Physics and Astronomy, Tufts University, Medford, Massachusetts 02155, USA

(Received 15 December 2016; accepted 20 March 2017; published online 12 April 2017)

The change in surface resistivity due to the formation of nickel islands on gold(111) was studied by measuring the resistance of a thin film of Au as a function of Ni coverage, θ. Previous studies showed that the Au(111) herringbone reconstruction provides a template for the periodic growth of ordered islands. Ni islands grow radially until θ ≈ 0.3 ML, after which subsequent Ni atoms contribute primarily to a second layer. Since Ni atoms on Au(111) grow in ordered nanoclusters, a nonlinear dependence of resistance on θ might be anticipated. Our results, however, show a linear dependence for Ni atoms in the first layer, as if they were independent point scatterers. Above θ ≈ 0.3 ML, there is little change in resistivity, which we attribute to Ni atoms in the second layer making no significant contribution to the resistivity. Although we did not directly image the islands, our results are consistent with the growth model and structures previously observed with scanning tunneling microscopy. Our results serve as an indirect probe of the growth kinetics of this system, as well as determining the contributions of Ni islands to the surface resistivity of the Au film. *Published by AIP Publishing.* [http://dx.doi.org/10.1063/1.4979846]

I. INTRODUCTION

In this paper, we present results on the surface resistivity contributions of ordered nanometer-scale Ni islands on a Au(111) substrate. Measurements of surface resistivity—the contribution of surface defects or impurities to the electrical resistivity of a thin metal film—offer insight into a wide variety of phenomena including electromigration,[1,2] electronic friction,[3–5] and vibrational spectroscopy.[6–8] From an applications standpoint, effects of surface resistivity have been shown to be important in studies of adsorbate effects on carbon nanotubes[9] and metallic nanowires[10] and may provide information on surface electronic properties relevant to nanoscale charge transfer for energy harvesting.[11] Surface resistivity can also be used as a probe to indirectly measure adsorption kinetics and thin film growth, which may prove useful for other works that involve the Au/Ni system, such as recent work on microelectromechanical system (MEMS) switches.[12]

As first proposed by Fuchs, and later Sondheimer, surface resistivity is due primarily to the diffuse scattering of conduction electrons at the surface and can result from anything that breaks the translational symmetry of the ideal surface, including defects, adsorbates, and surface phonons.[13,14] The current theory for adsorbate-induced changes in resistivity comes from Persson and Volokitin[15–17] and is based on the idea that adsorbates create an impurity potential, contributing to electrical resistivity by scattering conduction electrons.[18] Assuming randomly distributed non-interacting adsorbates, the change in surface resistivity of the film, $\Delta\rho$, can be related to the surface coverage of adsorbates, θ, by the following equation:

$$t\Delta\rho = \frac{3}{16}\ell_B\rho_B\Sigma n_s\theta, \tag{1}$$

where t is the sample thickness, ℓ_B is the bulk mean free path, ρ_B is the bulk resistivity, Σ is the effective scattering cross section per adsorbate, and n_s is the substrate's atomic surface density.[19]

If the scattering cross section Σ is independent of coverage, Equation (1) predicts a linear relationship between $\Delta\rho$ and θ, and such a relationship has been observed in a number of systems.[6,18,20–23] Other systems, however, show a nonlinear dependence, which can be attributed to nonrandom adsorption and/or significant interadsorbate interactions. Examination of the nonlinear dependence of resistivity on coverage can grant valuable insight into the presence of different chemical species or adsorption sites and interactions that alter the scattering cross section, surface morphology, and growth kinetics.[19,23–25] For nonmetallic adsorbates, it is generally observed that surface resistivity arises only from the first adsorbed layer, in which the adsorbates are in direct contact with the substrate.[23–26] Subsequent adsorbed layers do not contribute because they do not interact significantly with the substrate's conduction electrons.

The available literature on metallic adsorbate effects on surface resistivity is limited. All of the experiments on metallic adsorbates on metals show that in the sub-monolayer coverage range, the adsorbates behave as diffuse scattering centers and lead to an increase in the resistivity, though the exact monolayer coverages are not well quantified.[2,21,22,27–29] Two experiments that looked at Ag deposited on Ag and Cu on Cu found surface resistivity to increase linearly with coverage until the point when adatoms begin to increase the film thickness, after which a plateau, and sometimes a

a)Author to whom correspondence should be addressed. Electronic mail: roger.tobin@tufts.edu

decrease, in surface resistivity was observed.[21,22] Schumacher and Stark found that the surface resistivity contribution per additional Ag adatom decreases with increasing deposition temperature: an effect attributed to sufficient adatom mobility, which leads to the formations of islands with an effective cross section *lower* than that of the isolated adatoms.[22] For hetero-deposition systems, In and Ga deposited separately on both Ag and Au, Schumacher *et al.* found the scattering cross section of additional atoms to be *larger* for foreign adatoms when compared to deposition of the same adatoms as the substrate.[22]

In this work, we examine the surface resistivity of a Au(111) thin film as sub-monolayer coverages of Ni are deposited. When cleaned and annealed, the Au(111) surface configures into the herringbone reconstruction,[30–32] which is shown schematically in Figure 1(a). The herringbone reconstruction is composed of alternating fcc and hcp regions, 3.8 nm and 2.5 nm wide, respectively,[32] with surface atoms between these regions occupying bridge-sites that scanning tunneling microscopy (STM) images show as ridges ~0.02 nm high.[30,31] These ridges change the direction by 120° every ~14 nm due to this alternating stacking, leading to the characteristic zig-zag pattern and the formation of "elbows."[30]

Using scanning tunneling microscopy, Chambliss, Wilson, and Chiang demonstrated that Ni islands nucleate and grow at the elbows of the Au(111) herringbone reconstruction, leading for low Ni coverage to an ordered array of single-layer nanometer-scale Ni islands. Second-layer growth begins at a Ni coverage of approximately 0.3 ML.[31] Figures 1(b)–1(e) show schematically how the islands grow at the elbows of the reconstruction with increasing Ni coverage. Chambliss *et al.*

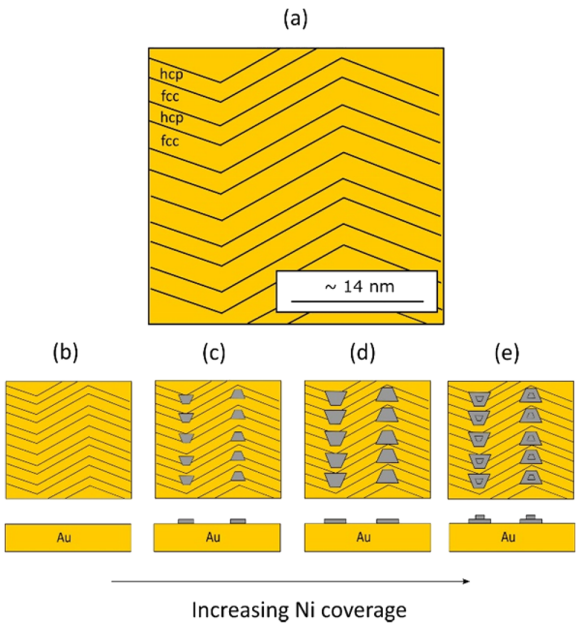

FIG. 1. Schematic representation of Ni island growth on Au(111) based on STM images in Refs. 34 and 43 and growth details from Ref. 31. The islands preferentially nucleate at the elbows of the herringbone reconstruction. ((a) and (b)) Clean Au(111) surface and the herringbone reconstruction. (c) Small islands begin to form at the elbows of the reconstruction. (d) As more Ni is deposited on the surface the islands grow outwardly. (e) At a certain coverage, the islands form a second layer before filling in the first layer.

suggest that there is a local distortion of an electronic or atomic structure that leads to the capturing of Ni atoms diffusing on the surface, which then serve as nucleation points for the formation of larger islands.[30] Subsequent STM studies have refined this picture. Meyer *et al.* found that the islands initially form through a two-step process of Ni atom place exchange with Au substrate atoms at the herringbone elbows, followed by subsequent aggregation of additional Ni atoms.[33] Cullen and First found topographical variations within the islands deposited at room temperature (RT), suggesting intermixing of Ni and Au atoms, with intermixing increasing as annealing and deposition temperatures rise above 350 K.[34] Later studies by Wang *et al.* and Therrien *et al.* have found Ni/Au(111) to be an interesting system to use as a periodic template for studies of the control of catalytic reactions in single atom alloys (SAA) and in studies of quantum effects observed in molecular hydrogen.[35,36]

Because many of the assumptions underlying Eq. (1) do not apply, the Ni/Au(111) system offers an interesting opportunity to extend our understanding of surface resistivity. Except at the very lowest Ni coverage, the Ni atoms are not well modeled as randomly distributed, non-interacting entities. Instead they form an ordered array of tightly packed two-dimensional crystalline islands, which could well lead to a nonlinear variation of $\Delta\rho$ with θ. Schumacher and Stark posited that the nonlinear variation of $\Delta\rho(\theta)$ observed at high coverages for Ag on Ag was due to the additional Ag atoms congregating into islands and possessing a smaller scattering cross section than independent Ag atoms.[22] For Ni on Au, second-layer adsorption begins at coverages above about 0.3 ML,[31] and since the first-layer Ni forms metallic islands, it is unclear to what extent the gold conduction electron wavefunctions extend through the island, and therefore whether to expect a surface resistivity contribution from the second-layer Ni. Somewhat surprisingly, we observe results consistent with more typical adsorption systems: A linear dependence of $\Delta\rho$ on θ for first-layer adsorption and essentially no contribution from the second-layer Ni.

II. EXPERIMENTS

The substrates were commercial 150 nm thick × 1 cm × 1 cm epitaxial Au(111) films on mica.[37] Contact pads (50 nm Ag on top of 10 nm Cr) were deposited *ex situ* under high vacuum on the corners for electrical contacts and in the middle of one edge for thermocouple attachment. The sample was then attached to a custom sample mount described elsewhere.[38] Wires were connected to the contact pads using colloidal silver paint[39] to enable resistivity and temperature measurements. The sample was transferred into an ultra-high vacuum chamber (UHV, base pressure 7×10^{-11} Torr), where the remainder of processing and measurement was completed. The sample was cleaned by Ar^+ sputtering (500 eV, ~7 μA/cm^2) and then annealed at 573-773 K for 10 min. Annealing is discussed in greater detail below. The sputtering/annealing process was repeated until no contaminants were detectable with Auger electron spectroscopy (AES). By comparing the background noise to the C signal, the maximum contaminant coverage is estimated to be 0.01 ML.

The herringbone reconstruction, which is essential to the growth of Ni nano-islands, is well established to be the equilibrium state of the clean Au(111) surface.[34,40] Following sputtering, our samples were annealed to enable the surface to equilibrate. Low-energy electron diffraction (LEED) observations did not exhibit distinct spots, but a clear ring showed that the surface was well-oriented, and periodic intensity variations within the ring indicated some degree of azimuthal ordering. There were no visually observable changes between samples held at RT after sputtering and those annealed at temperatures from 573 to 773 K for 10 min, suggesting that on these thin-film samples there is sufficient surface atom mobility for equilibration to occur even at RT, consistent with other reports.[34] We did not have the capability to establish directly the presence of the reconstruction or to determine the presence, size, or structure of the Ni nano-islands. The consistency of our observed coverage dependence of the surface resistivity with the growth process reported from STM experiments, however, provides strong indirect evidence that the desired structures were present.

An ac four-terminal technique was used to measure the film's sheet resistance, using the van der Pauw method for a square geometry, with contacts at the corners.[41,42] A 2.0 mA rms current modulated at 3 kHz was supplied to two adjacent corners, and the corresponding ac voltage was measured across the other two. Based on the comparison of the measured sheet resistance, $R_s^{measured} \approx 100\ \mathrm{m\Omega}/sq$, with that expected for pure Au, $R_s^{pure\,Au} \approx 150\ \mathrm{m\Omega}/sq$, we estimate that the absolute resistivity measurements have an uncertainty of roughly 50%, due to a combination of uncertainty in the sample thickness, especially after sputtering, and errors due to the non-negligible size and lack of ideal symmetry of the contact pads. Since our primary interest is in the fractional *changes* in resistivity due to the growth of the Ni islands, these uncertainties do not significantly affect our conclusions.

Following annealing, sub-monolayer Ni was deposited by thermal evaporation from 99.99% purity Ni wire wrapped around a well-outgassed tungsten filament. The sample temperature was regulated at 296.1 ± 0.1 K. Under these experimental conditions, an ordered array of Ni nanoparticles is known to form.[30,31,33–36,43–45] During the deposition, the resistance was continuously monitored. Figure 2 shows a typical trace displaying the change in sheet resistivity before, during, and after the Ni deposition. After a desired change in resistivity (typically about 0.5%) was observed, or after a predetermined period of deposition, the deposition was halted, and an AES spectrum was acquired to determine the Ni coverage θ. This procedure was repeated 3-5 times per experimental run.

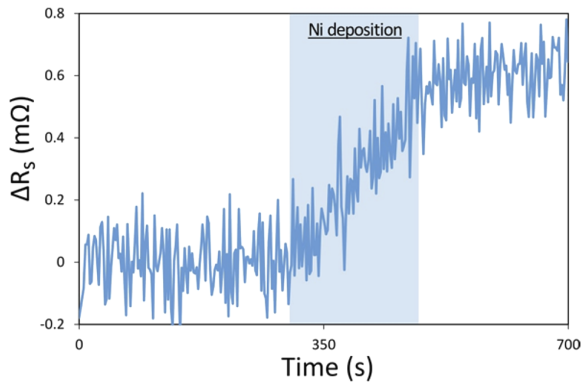

FIG. 2. Measured resistance change due to Ni deposition as a function of time. Ni deposition begins around 300 s and ends around 500 s, as indicated by the shaded region. At t = 0, $R_s \approx 100$ mΩ/sq.

Our measure of Ni coverage is based on a normalized ratio of the Ni and Au Auger signals,

$$\xi = \frac{\frac{\sigma_{Au}}{\sigma_{Ni}}\,[\mathrm{Ni}]\,/\,[\mathrm{Au}]}{1 + \frac{\sigma_{Au}}{\sigma_{Ni}}\,[\mathrm{Ni}]\,/\,[\mathrm{Au}]}, \tag{2}$$

where [Ni] is the 848 eV peak-peak height and [Au] is the 239 eV peak-peak height. $\frac{\sigma_{Au}}{\sigma_{Ni}}$ is the ratio of Auger cross sections for pure Au and pure Ni, determined from the ratio of [Au]/[Ni] measured in our system for pure Au and pure Ni taken under identical conditions. In the simple approximation that the Auger signal comes only from the topmost atomic layer and that Ni forms a single layer on Au, the Ni coverage θ is simply equal to the Auger ratio ξ. At the low coverages of interest, we found AES to be more sensitive than our commercial film thickness monitor. For accurate coverage determination, however, the AES signals must be corrected for finite electron penetration depth and two-layer Ni growth, as we discuss below.

After each experimental run, the sample was sputtered to remove the Ni and annealed to restore the equilibrium Au(111) surface structure. Naturally the repeated sputtering cycles gradually reduced the thickness of the sample, resulting in both higher clean-sample sheet resistance and higher fractional resistance changes upon Ni deposition. After several such cycles, the film became visibly transparent. Typically a given Au substrate could be used for 5-10 Ni depositions before it became too thin and nonuniform for reliable measurements. A new sample would then be installed and the process repeated. As we describe below, we are able to correct to a considerable degree for the changes in measured surface resistivity caused by the variations in sample thickness. Nevertheless, residual run-to-run and sample-to-sample variations constitute the dominant source of noise in our data. For clarity, we first present data from two successive runs on the same sample, before presenting the complete set of data (13 experimental runs on 4 samples).

III. RESULTS AND ANALYSIS

Figure 3(a) presents the adsorbate-induced sheet resistance change ΔR_s, as a function of Auger ratio ξ for two data sets collected from the same sample. It is clear from this figure that in both data sets, ΔR_s increases rapidly with ξ until $\xi \sim 0.3$–0.4; above this ξ value, ΔR_s plateaus as ξ increases. Scanning tunneling microscope observations of Chambliss *et al.* show that the second layer growth occurs after $\theta \approx 0.3$ ML.[31] Since for low coverage $\xi \approx \theta$, a qualitative interpretation of Fig. 3(a) is that the plateau corresponds to the start of second-layer growth, and that only the first-layer Ni contributes to surface resistivity, with negligible contribution from the second layer. As we show below, a more detailed analysis supports this interpretation. In addition to providing

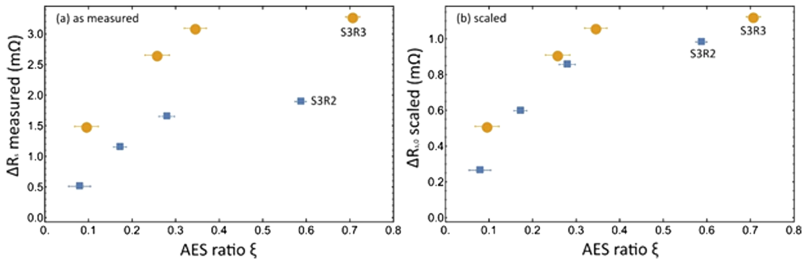

FIG. 3. Changes in sheet resistance ΔR_s, as a function of AES ratio ξ. (a) As measured values. (b) $\Delta R_{s,0}$ scaled for sample thinning. Error bars are determined from the noise levels in the individual AES and R_s measurements. Uncertainty in ΔR_s is smaller than the size of the data symbols.

new information about the surface resistivity contribution of the Ni nano-islands, the abrupt change seen in Fig. 3(a), at the same coverage at which second-layer growth is known to begin, provides strong indirect evidence that such nano-islands are in fact forming in our experiment.

The two data sets shown in Fig. 3(a) exhibit the same general shape, but the ΔR_s values are consistently higher for the later data set (S3R3). The value of R_s before Ni deposition was also higher for that data set. We attribute these differences primarily to thinning of the sample during sputtering. Similar behavior was observed on all of the samples studied. To allow data from different runs and different samples to be compared, we calculate a scaled value of ΔR_s that represents the change in sheet resistance that *would have been* observed if the sample were at its original thickness. Our scaling is based on the observation that in all plausible models of surface resistivity, the quantity $t\Delta\rho$ is independent of sample thickness t,[19,28,46] and on the fact that $R_s \sim \rho/t$, which leads to the conclusion that the quantity $t^2\Delta R_s$ should be independent of thickness. We do not have direct access to the thickness of the sample, but if the bulk resistivity of the sample does not change, the ratio of thicknesses is just the inverse of the ratio of the predeposition R_s values,

$$\frac{t}{t_0} = \frac{R_{s,0}}{R_s} \tag{3}$$

from which it follows that the scaled change in sheet resistance $\Delta R_{s,0}$ is related to the measured value by

$$\Delta R_{s,0} = \frac{t^2}{t_0^2}\Delta R_s = \frac{R_{s,0}^2}{R_s^2}\Delta R_s. \tag{4}$$

Here R_s is the sample's sheet resistance measured at RT, ΔR_s is the measured change in the sample's resistance, and the naught subscripts represent values when the sample is new. Figure 3(b) is the result of applying this scaling to the data in Fig. 3(a), and it can be seen that the scaled ΔR_s values fall much more nearly on a single curve.

To obtain a more accurate measure of Ni coverage θ from the AES ratio ξ, we take into account the attenuated but nonzero AES signal from subsurface atoms and the possibility of second-layer Ni adsorption. We use experimental values of the inelastic mean-free-path λ for both incident and Auger electrons in both Ni and Au to estimate the strength of the Auger signal[47] from (1) Au covered by Au, (2a) Au covered by one or (2b) two layers of Ni, and (3) Ni covered by Ni, as shown schematically in Fig. 4.

To determine the Ni coverage corresponding to a measured AES ratio ξ, we then need a model for the growth of the Ni film specifying the amount of first- and second-layer Ni at each coverage value. Motivated by the STM data of Chambliss *et al.*[31] and Trant *et al.*[43] who found AES coverage estimates agree well with coverage values determined with STM images, we assume a simple model in which Ni forms a single layer up to a threshold coverage θ_T, and above that threshold Ni atoms stick as a second layer with probability P_2, and in the first layer with probability $(1 - P_2)$, with no intermixing of Ni and Au,

$$\theta_1 = \begin{cases} \theta & for \quad \theta \le \theta_T \\ (1-P_2)\,\theta + \theta_T P_2 & for \quad \theta \ge \theta_T \end{cases}, \tag{5a}$$

$$\theta_2 = \begin{cases} 0 & for \quad \theta \le \theta_T \\ P_2\,(\theta - \theta_T) & for \quad \theta \ge \theta_T \end{cases}, \tag{5b}$$

$$\theta = \theta_1 + \theta_2. \tag{5c}$$

Here θ_1 represents the entire area covered by at least one layer of Ni and θ_2 represents the area covered by two layers of Ni, shown in Fig. 4. The values of θ_T and P_2 are not well known, and we treat them as adjustable parameters, but STM measurements suggest $\theta_T \sim 0.3$ *ML* and $P_2 \sim 1$.[31] The model makes sense only as long as $\theta_1 \le 1$ and $\theta_2 \le \theta_1$. Subject to these constraints, the growth model in combination with the correction for the electron inelastic mean free path makes it possible to determine the Ni coverage from the Auger ratio ξ.

We take a self-consistent approach to determining simultaneously the growth model parameters θ_T and P_2, and the relative contributions to the surface resistivity of first- and second-layer Ni. Motivated by the shape of the curves in Fig. 3, we begin with the simplest model of the surface resistivity: that only the first-layer Ni contributes and that the scattering cross section per Ni atom is independent of coverage,

$$\Delta R_s = \alpha\theta_1(\theta, \theta_T, P_2). \tag{6}$$

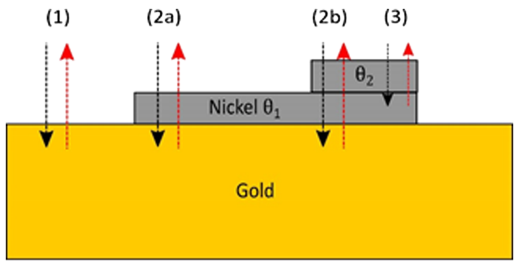

FIG. 4. Scenarios where λ affects AES electrons: (1) gold covered by gold, (2a) gold covered by one or (2b) two layers of nickel, and (3) nickel covered by nickel. The arrows represent the path of the AES electrons. Note: θ_1 represents all areas covered by at least one layer of Ni and θ_2 represents all areas covered by two layers of Ni.

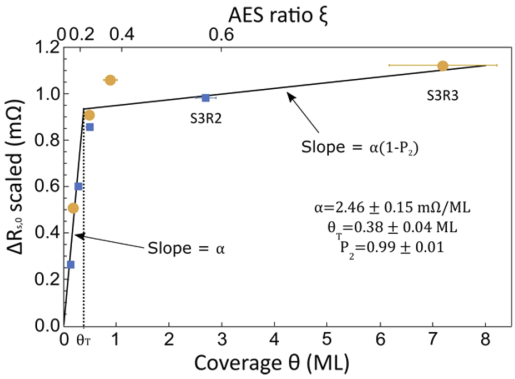

FIG. 5. Best fit data for scaled and mean free path corrected data, for the data shown in Fig. 3.

To estimate the values of the three unknown parameters θ_T, P_2, and α, we carried out nonlinear least-squares fits to the data shown in Fig. 3, and also to a larger set of 13 separate Ni deposition runs on four separate but nominally identical substrates.

Figure 5 displays the best fit of this model to the data from Fig. 3(b). The best-fit parameters were $\alpha = 2.46 \pm 0.15$ mΩ/ML, $\theta_T = 0.38 \pm 0.04$ ML, and $P_2 = 0.99 \pm 0.01$. The primary contribution to uncertainty came from the Auger signals, which was estimated by the signal noise. Uncertainty in α, θ_T, and P_2 was found by randomly varying the ξ values of our data points within their uncertainties and looking at the resulting scatter in the best fit parameters. The results are consistent with a model of surface resistivity in which the first-layer Ni atoms act as independent point scatterers, and the second-layer Ni atoms do not contribute to the resistivity, and with a growth model of first-layer growth up to a Ni coverage of about 0.4 ML followed by second-layer growth at higher coverage.

The coverage axis in Fig. 5 extends to much higher θ values than are reasonable for our growth model, and these large coverage values should not be taken literally. They arise because for Auger ratios above $\xi = 0.5$, where most of the surface is Ni-covered, the conversion from ξ to θ becomes highly sensitive to the parameters and details of the model. For purposes of our analysis, however, the important aspects of the fit are the transition coverage θ_T, the slope of the line

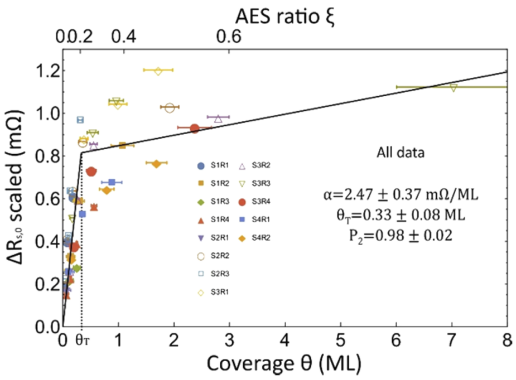

FIG. 6. Global fit for data corrected for sample thinning and the inelastic mean free path of electrons. Data point names S#R# refer to sample number and run number; thus, S3R2 refers to the second Ni deposition experiment on Au substrate #3.

at lower coverages, and the nearly flat slope of the resistance change for coverages above that value. These characteristics are relatively insensitive to the details of the growth model at higher coverages.

Figures 3 and 5 present data from two experimental runs on a single Au substrate. Figure 6 presents the same analysis for all of our runs—a total of 13 separate Ni depositions on 4 different Au substrates. A global fit of the model to all the data gives the best fit values of $\alpha = 2.47 \pm 0.37$ mΩ/ML, $\theta_T = 0.33 \pm 0.08$ ML, and $P_2 = 0.98 \pm 0.02$. When comparing all the data, uncertainty was dominated by scatter due to run-to-run variations. Uncertainty in the fitted parameters was estimated by examining the variation in χ^2 values and visual examination of the corresponding fits. The values of α and P_2 are nearly identical to those given in Fig. 5. The global fit value of θ_T is slightly lower and in fact closer to the transition coverage for second-layer growth reported in STM studies,[31] but within the estimated uncertainties. In three of the depositions included in Fig. 6 (S3R4, S4R1, S4R2), the substrate was annealed only by a brief flash to 573 K before Ni deposition, to avoid contamination and damage to the electrical contacts. These data were not distinguishable from cases when the substrate was annealed at higher temperatures and for longer times, suggesting that for these thin film samples the Au surface reconstructs at relatively low temperatures.

Our data show that for Ni coverages greater than θ_T, the surface resistivity continues to increase slightly, but at a rate only 1%-2% as large as at lower coverages. In our model we have attributed that increase to a small probability of first-layer deposition. It is also possible, however, to attribute it to a small surface resistivity contribution from the second-layer Ni or to some combination of the two effects. Our data do not provide a basis for separating the two effects. It is unmistakable, however, that once second-layer growth begins the rate of surface resistivity increase is reduced by nearly two orders of magnitude.

The parameter α in our model corresponds to the surface resistivity contribution per additional first-layer Ni atom. Through Eq. (1), we can use our best-fit value $\alpha = 2.47 \pm 0.37$ mΩ/ML in combination with known or estimated values for the surface density of unreconstructed Au(111) (1.387×10^{15} atoms/cm^2), the RT bulk mean free path of Au(111) (37.7 nm),[48] and the nominal thickness and RT sheet resistance of our substrates (150 nm and 100 mΩ/sq, respectively) to estimate the scattering cross section per first-layer Ni atom: $\Sigma \approx 4.2 \pm 1.7$ Å^2. Compared to other systems that have been studied, this is a relatively small value. For reference, O on Cu (111) has $\Sigma \approx 19$ Å^2 and Ag on Ag(111) has $\Sigma \approx 14$ Å^2.[16]

At low coverages, deposition of metallic adatoms on the smooth surface of a metal film generally increases the film's resistance due to scattering of conduction electrons,[21,22,28] as we observe. At some point, however, the deposition of a conducting film on top of the original film would be expected to decrease the system's resistance by providing a parallel conduction path, as has been observed with Ag on Ag.[22,26] To check whether the leveling off of the resistivity-coverage curve that we observe could be due to the transition between these

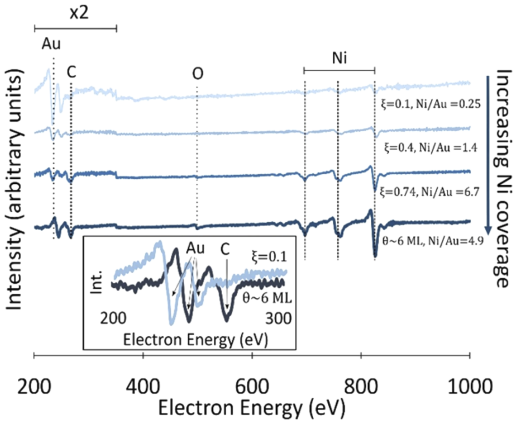

FIG. 7. AES spectra for different Ni coverages, with the largest Ni coverage at the bottom. For sub-monolayer coverage, the Au peak decreases and the Ni peak increases monotonically. An increase in the Au peak is observed after ~6 ML of Ni is deposited. The Ni/Au ratios reported in curve labels are peak height ratios, uncorrected for Auger cross section. Inset shows the Au peaks for the lowest and highest Ni coverages. The Au peak for multiple ML coverage appears to be near the average of the two peaks for the low coverage spectrum, which could be an effect of alloying.

two limits, we carried out an experiment in which a relatively large amount of Ni was deposited (~6 ML as measured by a quartz crystal microbalance). We found that the film resistance continued to increase, and AES spectra showed a significant Au peak, suggesting that a Ni-Au alloy is forming, consistent with other studies.[12,49–52] This experiment confirms that the plateau for $\theta > \theta_T$ seen in our low-coverage data is related to a lack of scattering from the second-layer Ni, not to the onset of parallel conduction in a continuous Ni layer.

This experiment, however, together with STM observations that suggest intermixing of Au and Ni atoms,[34] raises the question of whether our model, which ignores intermixing, adequately represents the system. Both the available literature and our data indicate that intermixing is negligible at RT at the low coverages studied here.[31,43] Combined STM and AES studies have found that the two methods of coverage determination give consistent results over the coverage range in which island formation occurs.[31,43] In our measurements seen in Fig. 7, we found that for sub-monolayer Ni coverages, the Au AES signal decreases monotonically with increasing Ni coverage. For the 6 ML Ni deposition, however, we see an *increase* in the Au AES signal, accompanied by a qualitative change in the AES line shape from the characteristic Au double peak to a single peak at an intermediate energy, as shown in the inset. We interpret this change in the spectrum as due to the formation of a surface alloy, and its absence at sub-monolayer coverages as support for our assumption that intermixing is at most a minor effect.

At very low Ni coverages, $\theta \sim 0.002$ ML, Meyer *et al.* found depressions in the Au(111) surface with STM, which they interpret as indicating substitutional Ni at the elbows of the herringbone reconstruction that provide the nucleation sites for subsequent island growth.[33] It is certainly plausible that these substitutional Ni atoms would exhibit a different scattering cross section from Ni deposited on top of the Au surface, but our measurements are not sensitive enough to distinguish the effect due to such a small amount of Ni.

IV. DISCUSSION

The current theoretical understanding of surface resistivity is based almost entirely on a model of independent, randomly distributed point scatterers interacting directly with the metal substrate.[15–17] This model leads to the prediction of a linear dependence of resistivity on coverage, as expressed in Eq. (1), and to the expectation that second- and higher-layer adsorbates will have little or no effect. This model works well for adsorption systems such as CO on Cu(100)[6] and O on Cu(100),[18] in which repulsive interactions keep the adsorbates separated. The linearity extends even to high coverages where the formation of ordered structures might be expected to lead to deviations from linearity.[19] For S on Cu(100), the resistivity levels off at high S coverages, an effect attributed to interactions between the adsorbed atoms that strongly suppress the scattering cross section.[18]

Because the adsorbates directly interact with the conduction electrons in the metal, adsorbate-induced changes in surface resistivity are expected to be a first layer effect. Hsu, McCullen, and Tobin simultaneously studied surface resistivity and reflectance changes for formic acid on Cu(100) and found that only adsorbates in the first layer contribute to surface resistivity while multilayer growth showed a reflectance change.[23] Grabhorn, Otto, Schumacher, and Persson exposed Ag films to ethylene, ethane, and benzene and found the surface resistivity to increase linearly until a coverage of about 1 ML, after which no changes in surface resistivity were measured.[26] Other resistance change studies of sub-monolayer depositions of metal adsorbates indicate that there is a coverage where additional adsorbates no longer contribute to the resistance; however, the exact coverage where this occurs is not well quantified.[2,21,22,27]

In the present experiment, for the first-layer Ni, we observe the linear dependence on coverage predicted for non-interacting, random scatterers, even though those assumptions are strongly violated: the Ni atoms are clustering to form an ordered array of close-packed islands with interatomic spacing comparable to the Fermi wavelength of the Au conduction electrons. A possible clue to this surprising result may be found in the relatively low scattering cross section ($\Sigma \approx 4.2 \pm 1.7$ Å^2) per Ni atom. If each atom is a weak scatterer, it could make sense that the total diffuse scattering is simply proportional to the area of the surface covered by Ni. This interpretation is supported by the work of Schumacher *et al.* with Ag on Ag, a comparatively strong scatterer, where they explain the resistance change behavior as due to collective island effects on the scattering cross section.[22] Future work could include looking at other adsorbates such as Co, Fe, and Ti that also form nanoislands.[53–55] An *ab initio* calculation of induced resistivity of magnetic atoms on the surface of a free-electron metal by Trioni *et al.* found that the scattering cross section can vary widely for different elements, depending on the relationship between the adatom's induced density of states and the Fermi level of the substrate.[56]

V. CONCLUSIONS

We have determined for the first time surface resistivity contributions of first and second layer Ni nanoislands grown

on Au(111). Our results are consistent with the growth mode previously identified in STM studies, with Ni growing primarily in the first layer up to a critical coverage $\theta_T = 0.33 \pm 0.08$ ML, after which island growth is primarily second layer. For first-layer growth, the surface resistivity varies linearly with coverage, consistent with a model of non-interacting random point scatterers, even though the atoms are instead forming an ordered array of compact islands. We speculate that the lack of detectable interaction effects may be due to the small scattering cross section of each Ni atom. Above θ_T there is almost no additional increase in surface resistivity, indicating that the second-layer Ni has negligible effect. Evidently there is little penetration of the Au electron wavefunctions into the Ni islands.

Our results also show that surface resistivity can provide a useful indirect probe of thin film growth through its sensitivity to surface coverage and ability to distinguish first-layer from second- and higher-layer growth.

ACKNOWLEDGMENTS

J.I.C. gratefully acknowledges support from a John A. Burlingame Fellowship from Tufts University.

[1]M. F. G. Hedouin and A. F. Rous, Phys. Rev. B **62**, 8473 (2000).
[2]S. M. Rossnagel and T. S. Kuan, J. Vac. Sci. Technol., B: Microelectron. Nanometer Struct. **22**, 240 (2004).
[3]B. N. J. Persson, J. Chem. Phys. **98**, 1659 (1993).
[4]J. B. Sokoloff, Phys. Rev. B **52**, 5318 (1995).
[5]A. Dayo, W. Alnasrallah, and J. Krim, Phys. Rev. Lett. **80**, 1690 (1998).
[6]C. J. Hirschmugl, Y. J. Chabal, F. M. Hoffmann, and G. P. Williams, J. Vac. Sci. Technol., A **12**, 2229 (1994).
[7]C. J. Hirschmugl, G. P. Williams, B. N. J. Persson, and A. I. Volokitin, Surf. Sci. **317**, L1141 (1994).
[8]C. L. A. Lamont, B. N. J. Persson, and G. P. Williams, Chem. Phys. Lett. **243**, 429 (1995).
[9]G. U. Sumanasekera, C. K. W. Adu, S. Fang, and P. C. Eklund, Phys. Rev. Lett. **85**, 1096 (2000).
[10]C. Z. Li, H. Sha, and N. J. Tao, Phys. Rev. B **58**, 6775 (1998).
[11]Y. S. Zhou, S. M. Li, S. M. Niu, and Z. L. Wang, Nano Res. **9**, 3705 (2016).
[12]Z. Y. Yang, D. J. Lichtenwalner, A. S. Morris, J. Krim, and A. I. Kingon, J. Microelectromech. Syst. **18**, 287 (2009).
[13]K. Fuchs, Math. Proc. Cambridge Philos. Soc. **34**, 100 (1938).
[14]E. H. Sondheimer, Adv. Phys. **1**, 1 (1952).
[15]A. I. Volokitin and B. N. J. Persson, Phys. Rev. B **52**, 2899 (1995).
[16]B. N. J. Persson, Chem. Phys. Lett. **197**, 7 (1992).
[17]B. N. J. Persson, Surf. Sci. **269**, 103 (1992).
[18]R. G. Tobin, Surf. Sci. **524**, 183 (2003).
[19]R. G. Tobin, Surf. Sci. **502**, 374 (2002).
[20]C. L. Hsu, E. F. McCullen, and R. G. Tobin, Chem. Phys. Lett. **316**, 336 (2000).
[21]M. Hein and D. Schumacher, J. Phys. D: Appl. Phys. **28**, 1937 (1995).
[22]D. Schumacher and D. Stark, Surf. Sci. **123**, 384 (1982).
[23]C. L. Hsu, E. F. McCullen, and R. G. Tobin, Surf. Sci. **542**, 120 (2003).
[24]C. Liu and R. G. Tobin, J. Chem. Phys. **128**, 244702 (2008).
[25]C. Liu and R. G. Tobin, J. Chem. Phys. **126**, 124705 (2007).
[26]H. Grabhorn, A. Otto, D. Schumacher, and B. N. J. Persson, Surf. Sci. **264**, 327 (1992).
[27]P. Y. Zheng, R. P. Deng, and D. Gall, Appl. Phys. Lett. **105**, 131603 (2014).
[28]D. Schumacher, in *Springer Tracts In Modern Physics*, Surface Scattering Experiments with Conduction Electrons Vol. 128 (Springer, Berlin, 1993).
[29]J. S. Chawla and D. Gall, Appl. Phys. Lett. **94**, 252101 (2009).
[30]D. D. Chambliss, R. J. Wilson, and S. Chiang, Phys. Rev. Lett. **66**, 1721 (1991).
[31]D. D. Chambliss, R. J. Wilson, and S. Chiang, J. Vac. Sci. Technol., B: Microelectron. Nanometer Struct. **9**, 933 (1991).
[32]W. Chen, V. Madhavan, T. Jamneala, and M. F. Crommie, Phys. Rev. Lett. **80**, 1469 (1998).
[33]J. A. Meyer, I. D. Baikie, E. Kopatzki, and R. J. Behm, Surf. Sci. **365**, L647 (1996).
[34]W. G. Cullen and P. N. First, Surf. Sci. **420**, 53 (1999).
[35]Z.-T. Wang, M. T. Darby, A. J. Therrien, M. El-Soda, A. Michaelides, M. Stamatakis, and E. C. H. Sykes, J. Phys. Chem. C **120**, 13574 (2016).
[36]A. J. Therrien, A. Pronschinske, C. J. Murphy, E. A. Lewis, M. L. Liriano, M. D. Marcinkowski, and E. C. H. Sykes, Phys. Rev. B **92**, 161407 (2015).
[37]Samples purchased from Structure Probe, Inc. Item Number 466PS-AB
[38]E. T. Krastev and R. G. Tobin, J. Vac. Sci. Technol., A **16**, 743 (1998).
[39]Silver Print II from GC Electronics Part No. 22–023.
[40]N. Takeuchi, C. T. Chan, and K. M. Ho, Phys. Rev. B **43**, 13899 (1991).
[41]L. J. v. d. Pauw, Philips Res. Repts. **13**, 1 (1958).
[42]I. Miccoli, F. Edler, H. Pfnur, and C. Tegenkamp, J. Phys.: Condens. Matter **27**, 223201 (2015).
[43]A. G. Trant, T. E. Jones, J. Gustafson, T. C. Q. Noakes, P. Bailey, and C. J. Baddeley, Surf. Sci. **603**, 571 (2009).
[44]H. Hannemann, C. A. Ventrice, T. Bertrams, A. Brodde, and H. Neddermeyer, Phys. Status Solidi A **146**, 289 (1994).
[45]C. A. Ventrice, T. Bertrams, H. Hannemann, A. Brodde, and H. Neddermeyer, Phys. Rev. B **49**, 5773 (1994).
[46]P. Wissmann and K. Muller, *Springer Tracts in Modern Physics* (Springer, 1975), Vol. 77.
[47]C. J. Powell and A. Jablonski, NIST Electron Inelastic-mean-free-path Database - Version 1.2 (National Institute of Standards and Technology, Gaithersburg, MD, 2010).
[48]D. Gall, J. Appl. Phys. **119**, 085101 (2016).
[49]F. L. Williams and M. Boudart, J. Catal. **30**, 438 (1973).
[50]J. Jacobsen, L. P. Nielsen, F. Besenbacher, I. Stensgaard, E. Laegsgaard, T. Rasmussen, K. W. Jacobsen, and J. K. Norskov, Phys. Rev. Lett. **75**, 489 (1995).
[51]L. P. Nielsen, F. Besenbacher, I. Stensgaard, E. Laegsgaard, C. Engdahl, P. Stoltze, K. W. Jacobsen, and J. K. Norskov, Phys. Rev. Lett. **71**, 754 (1993).
[52]M. B. Hugenschmidt, A. Hitzke, and R. J. Behm, Phys. Rev. Lett. **76**, 2535 (1996).
[53]A. Delga, J. Lagoute, V. Repain, C. Chacon, Y. Girard, M. Marathe, S. Narasimhan, and S. Rousset, Phys. Rev. B **84**, 035416 (2011).
[54]P. Carrozzo, F. Tumino, M. Passoni, C. E. Bottani, C. S. Casari, and A. L. Bassi, Surf. Sci. **619**, 77 (2014).
[55]T. H. Gentner, F. Scheurer, T. Detzel, and J. P. Bucher, Thin Solid Films **275**, 58 (1996).
[56]M. I. Trioni, H. Ishida, and G. P. Brivio, Phys. Rev. B **65**, 125413 (2002).